

## Article

# Lignin-Derived Ternary Polymeric Carbon as a Green Catalyst for Ethyl Levulinate Upgrading from Fructose

Dayong Yu <sup>1,2,†</sup>, Xiaofang Liu <sup>1,\*,†</sup>, Hangyu Luo <sup>1,2</sup>, Jinshu Huang <sup>2</sup> and Hu Li <sup>2,\*</sup>

<sup>1</sup> Guizhou Provincial Key Laboratory for Rare Animal and Economic Insects of the Mountainous Region, College of Biology and Environmental Engineering, Guiyang University, Guiyang 550005, China; yudayong19960128@163.com (D.Y.); luohygzzy@163.com (H.L.)

<sup>2</sup> State Key Laboratory Breeding Base of Green Pesticide & Agricultural Bioengineering, Key Laboratory of Green Pesticide & Agricultural Bioengineering, Ministry of Education, State-Local Joint Laboratory for Comprehensive Utilization of Biomass, Center for Research & Development of Fine Chemicals, Guizhou University, Guiyang 550025, China; gs.jshuang20@gzu.edu.cn

\* Correspondence: liuxfzap@163.com (X.L.); hli13@gzu.edu.cn (H.L.)

† These authors contributed equally to this work.

**Abstract:** Currently, the utilization of lignocellulose mainly focuses on the conversion of polysaccharide components to value-added chemicals, such as ethyl levulinate (EL). Lignin is an important component of lignocellulosic biomass that is often neglected. Herein, ternary polymeric carbon (TPC-S) was synthesized by polymerization of mixed monomers (4-methylphenol, 4-ethylphenol, and 4-propylphenol) derived from lignin and subsequent sulfonation, which was used as a heterogeneous catalyst for the transformation of fructose to EL. Through a series of characterization methods, it was illustrated that the prepared catalyst had a layered porous structure. The calculated carbon layer spacing is 0.413 nm, and the average pore size is 5.1 nm. This structure greatly increases the specific surface area (165.2 m<sup>2</sup>/g) of the catalyst, which makes it possible to introduce more -SO<sub>3</sub>H species in the process of sulfonation, thus furnishing EL with increased yield. The effects of reaction temperature, time, catalyst dosage, and fructose initial concentration on the production of EL were investigated. It was found that 70.3% EL yield was detected at 130 °C for 10 h. In addition, the catalyst had good stability and could obtain 65.6% yield of EL in the fourth cycle. The obtained catalyst has the advantages of low cost, easy preparation, and high catalytic efficiency, which is expected to achieve efficient utilization of lignin and provide a potential solution for the future production of EL.

**Keywords:** biomass conversion; ethyl levulinate; lignin; fructose; sulfonation



**Citation:** Yu, D.; Liu, X.; Luo, H.; Huang, J.; Li, H. Lignin-Derived Ternary Polymeric Carbon as a Green Catalyst for Ethyl Levulinate Upgrading from Fructose. *Catalysts* **2022**, *12*, 778. <https://doi.org/10.3390/catal12070778>

Academic Editor: John Vakros

Received: 15 June 2022

Accepted: 12 July 2022

Published: 14 July 2022

**Publisher's Note:** MDPI stays neutral with regard to jurisdictional claims in published maps and institutional affiliations.



**Copyright:** © 2022 by the authors. Licensee MDPI, Basel, Switzerland. This article is an open access article distributed under the terms and conditions of the Creative Commons Attribution (CC BY) license (<https://creativecommons.org/licenses/by/4.0/>).

## 1. Introduction

Lignocellulose, as one of the renewable sources of energy, is estimated to increase by approximately 120 billion tons annually worldwide [1]. However, such a large amount of lignocellulose faces the usual problem of not being used with high value. Most of it is disposed of by direct combustion or landfill, which not only produces large amounts of CO<sub>2</sub> to pollute the environment but also occupies living space [2]. Lignocellulosic biomass is calculated to be equivalent to 50 billion tons of fossil energy if fully utilized [3]. Therefore, improving its utilization efficiency is of great significance to economic growth, environmental friendliness, and social progress [4]. For example, lignocelluloses can be converted into fuels and fine chemicals by thermochemical conversion. The products obtained by its transformation involve various C5 (e.g., xylose, arabinose) and C6 (e.g., glucose, fructose, galactose, and mannose) sugars, and their derivatives such as furfural (FF), 5-hydroxymethylfurfural (HMF), levulinic acid (LA), 5-ethoxymethylfurfural (EMF), and ethyl levulinate (EL) [5–8]. EL, as a short-chain platform molecule, is widely used in various fields. Because of its unique flavor and appropriate viscosity, it is often used as a food flavoring agent and plasticizer [9]. In addition, it has a high energy density

(24.8 MJ/L), which can reduce the emission of toxic gases ( $\text{SO}_x$ ,  $\text{NO}_x$ ) when mixed with traditional diesel (<5 wt%) [10]. At the same time, it can improve the low-temperature fluidity of mixed diesel and give it better combustion efficiency [11]. EL is also used as the substrate for the synthesis of downstream products, such as  $\gamma$ -valerolactone obtained by the transfer hydrogenation of EL [12].

Currently, there are three main methods for preparing EL from biomass and its derivatives: (i) LA is directly esterified in ethanol, (ii) alcoholysis of furfuryl alcohol (FA), and (iii) multistep alcoholysis of biomass (e.g., cellulose, glucose, and fructose). Although LA and FA as raw materials can produce high-yield EL [13,14], the high price makes them unable to be widely used. Cellulose and glucose as substrates to produce EL can solve the problem of expensive raw materials, but the problem of low yield of target products still needs to be solved. However, fructose, as a cheap biomass-derived monosaccharide, is more easily converted to desired products. Therefore, the development of an appropriate acid to convert fructose into EL is a good choice.

In the system without a catalyst, EL can be obtained by high-temperature reactive distillation [15], but the energy consumption of the reaction process is too high, which is extremely unfavorable for obtaining EL from biomass in the future. In the traditional catalytic system, many inorganic liquid acids (e.g.,  $\text{H}_2\text{SO}_4$ , HCl, and  $\text{H}_3\text{PO}_4$ ) have been explored for the synthesis of EL [16,17]. However, the use of these acids will cause some unsatisfactory problems, such as equipment corrosion, cumbersome steps for separation and purification, lack of reusability, and increased costs. Therefore, recyclable heterogeneous catalysts are selected as alternatives. Thus far, many solid catalysts have been designed for the synthesis of EL, including modified zeolites [18], supported heteropoly acids, modified montmorillonite [19], sulfonic acid-based solid catalysts [9], etc. In the catalytic conversion of biomass and its derivatives to EL, many heterogeneous acids with high acidity are more prominent [20]. The sulfonic acid-based solid catalysts usually contain high acidity. For example, Wang et al. synthesized Zr-DBS solid catalyst containing a sulfonic group with sodium dodecyl benzene sulfonate and  $\text{ZrOCl}_2$ , which was used for the alcoholysis of FA to EL (95.27% yield) [21]. Guo et al. reported an aminosulfonated carbon and evaluated the alcoholysis/esterification properties of FA and LA [9]. Tian et al. prepared sulfonated attapulgite (ATTP) catalyst with ATTP as the support for the evolution of FA to EL [22]. However, considering the complex preparation process and high cost of these sulfonated precursors, these catalysts are not applicable for economic benefits, and thus the development of low-cost sulfonated carriers is of more practical significance. As cheap renewable energy sources in the biosphere, cellulose and hemicellulose can be upgraded to high-value products through chemical or biological transformation. However, lignin, as one of the main components of lignocellulose, faces the negative issue of difficult utilization [23].

In order to promote the effective application of lignin, in this study, a polymeric carbon catalyst (TPC-S) was synthesized through (1) polymerization and (2) sulfonation of three lignin derivatives under mild (80 °C) conditions. Furthermore, the TPC-S was used to study the reaction parameters of fructose-to-EL conversion. The optimal catalytic parameters were found to obtain 70.3% EL at 130 °C for 10 h. At the same time, the physicochemical characterization of TPC-S showed that it had an obvious layered porous structure. This allowed the catalyst to introduce more  $-\text{SO}_3\text{H}$  groups, resulting in higher acid density (5.32 mmol/g), which could be more effective for catalytic conversion of fructose to obtain EL.

## 2. Results and Discussion

### 2.1. Catalyst Characterization

FT-IR spectra of TPC and TPC-S were recorded in the range of 4000–500  $\text{cm}^{-1}$  (Figure 1a). The band at 3440  $\text{cm}^{-1}$  was attributed to  $-\text{OH}$  stretching vibration on benzene rings. The band near 2960–2870  $\text{cm}^{-1}$  was the C–H stretching vibration of methylene. This proves that aromatic monomers were polymerized successfully. The bands at 1620  $\text{cm}^{-1}$  and 1460  $\text{cm}^{-1}$  belonged to the C=O stretching vibration of carboxyl group and C=C stretching vibration of the aromatic ring, respectively. In addition, in the TPC-S catalyst,

the characteristic peak of S-phenyl stretching vibration appeared at  $1035\text{ cm}^{-1}$  [24], but it was not found in TPC. This indicated that  $-\text{SO}_3\text{H}$  was successfully grafted onto the benzene ring of TPC.

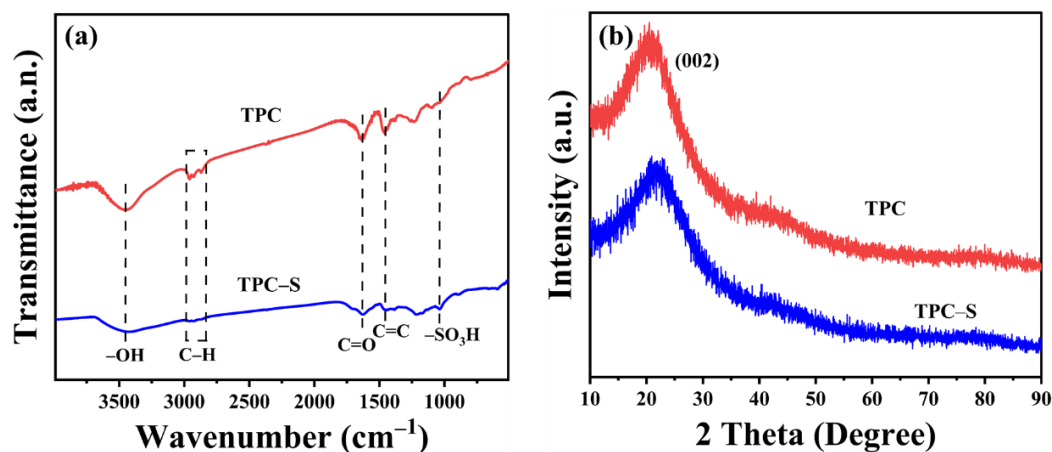


**Figure 1.** (a) FT-IR spectra and (b) XRD diffraction patterns of TPC and TPC-S.

Figure 1b shows the XRD diffraction patterns of TPC and TPC-S. A wide diffraction peak (002) at  $10\text{--}30^\circ$  was observed for TPC and TPC-S due to the amorphous structure of polymeric carbon derived from aromatic carbon. TPC-S prepared by sulfonation of TPC had no change except a decrease in peak intensity. This is because the concentrated  $\text{H}_2\text{SO}_4$  affects the structure of the chemical bonding of the biocarbon [25]. Generally, carbon with an amorphous structure is due to its disordered layered structure [26], indicating that the polymeric carbon is stacked by aromatic carbon layers. The carbon layer spacing of the catalyst was calculated by the Bragg formula, as shown in Table 1. The carbon layer spacing of TPC-S was 0.413 nm, slightly smaller than that of TPC (0.443 nm) because the introduction of  $-\text{SO}_3\text{H}$  reduced the distance between carbon layers. This further proved the successful introduction of  $-\text{SO}_3\text{H}$  into TPC.

**Table 1.** The distance between carbon layers of TPC and TPC-S.

Entry	Catalyst	$2\theta_{002}$ ( $^\circ$ )	$d_{002}$ (nm)
1	TPC-S	21.57	0.413
2	TPC	20.1	0.443

The XPS spectra of the unsulfonated sample (TPC) and sulfonated sample (TPC-S) were detected to identify the elemental composition (Figure 2). Figure 2a provides the C 1s, O 1s, and S 2p XPS signal bands of TPC and TPC-S, which showed peaks at 284 eV, 533 eV, and 169 eV, respectively. The S 2p signal band was not found in TPC. The C 1s fitting spectra of TPC-S (Figure 2b) showed four single peaks at 288.8 eV, 286.5 eV, 285.1 eV, and 284.4 eV, corresponding to  $-\text{COOH}$ , C-O, C-C, and aromatic carbon, respectively [27]. The O 1s peak of TPC-S could be deconvoluted into three components at 534.0 eV, 532.8 eV, and 531.5 eV, which were due to the C-OH of phenol and the S=O and S-OH of  $-\text{SO}_3\text{H}$ , respectively [28]. The S 2p XPS fitting spectra (Figure 2d) of TPC-S indicated the presence of  $\text{S}^{6+}$  (168.5 eV) in it [29]. These results indicated that  $-\text{SO}_3\text{H}$  was successfully grafted onto TPC after sulfonation with  $\text{H}_2\text{SO}_4$ .

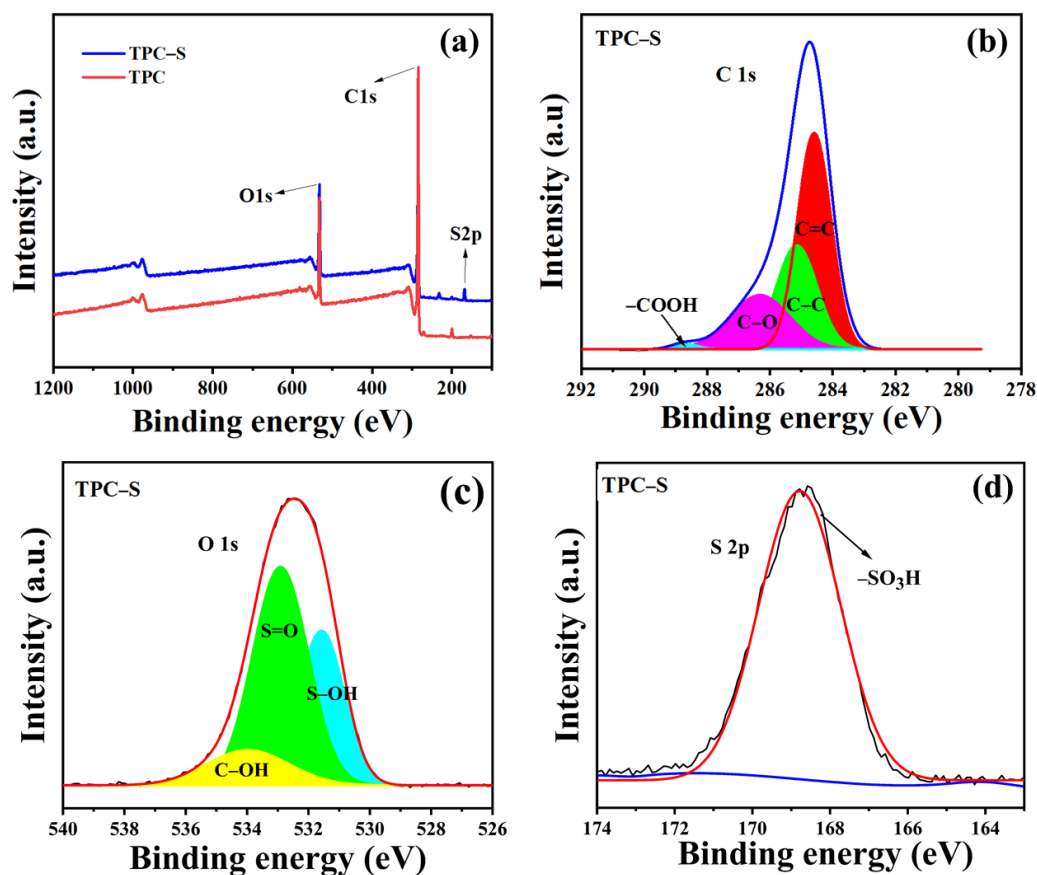


Figure 2. (a) XPS spectra of TPC and TPC-S, and (b) C 1s, (c) O 1s, and (d) S 2p XPS spectra of TPC-S.

The  $\text{NH}_3$ -TPD profile of TPC-S is shown in Figure 3. Two absorption peaks could be observed, one from 50 to 125 °C belonging to weak acid sites, and the other from 125 to 300 °C belonging to strong acid sites [30]. The peak areas of the two acid sites were fitted, and the corresponding acid densities were calculated to be 0.59 mmol/g and 4.73 mmol/g, respectively. Compared with other carbon carriers [9], the high acid density of TPC-S was due to the existence of a layered structure, which provided more sites for sulfonic group grafting [31].

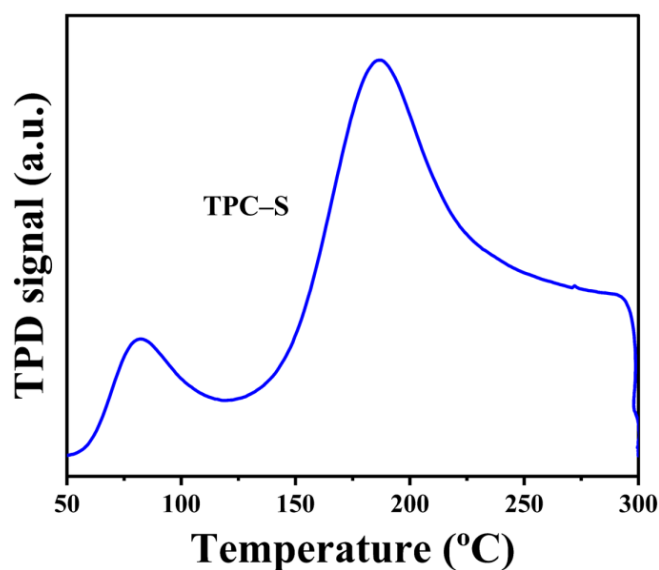
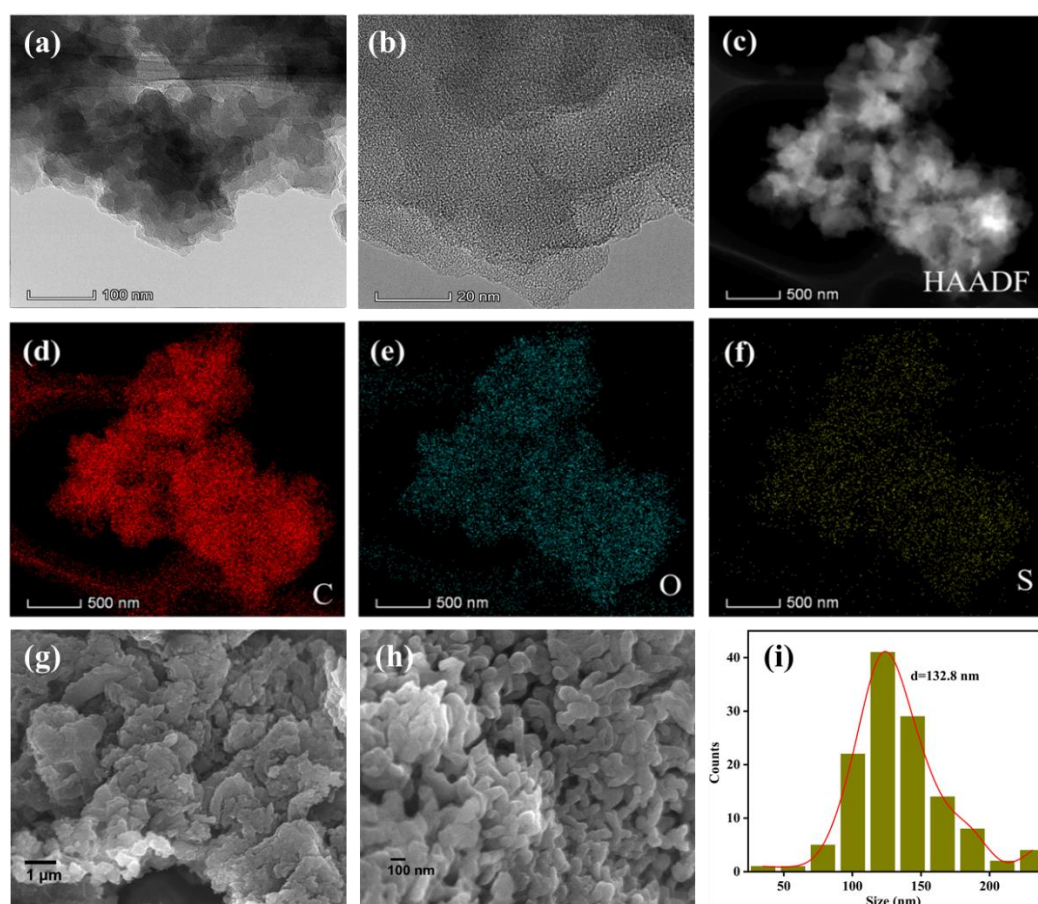


Figure 3. The  $\text{NH}_3$ -TPD curves of TPC-S.

The interior microstructure of TPC-S was observed by HR-TEM (Figure 4a,b). It could be seen that TPC-S is an amorphous structure without crystal form, which is consistent with the XRD results. The lamellar structure could be observed, further proving that TPC-S is stacked by aromatic carbon layers. The HAADF-STEM and element mapping diagram of TPC-S (Figure 4c-f) showed that the elements (C, O, and S) are evenly distributed on the TPC-S, signifying that the active sites ( $-\text{SO}_3\text{H}$ ) of the TPC-S are equally dispersed, which is more beneficial to the reaction.



**Figure 4.** (a,b) HR-TEM images of TPC-S; (c) HAADF-STEM image of TPC-S; (d) C, (e) O, and (f) S element mappings; and (g–i) SEM images of TPC-S.

The surface morphology of TPC-S, revealed by SEM images, is instead shown in Figure 4g–i. The catalyst surface is composed of many irregular particles (132.8 nm), and the evident porous structure is formed due to the release of CO and CO<sub>2</sub> gas during sulfonation. Overall, the layered porous structure of the catalyst provides more accessible sites for the reaction [32], thus promoting the whole conversion process.

Figure 5 shows the BET and BJH curves of TPC-S. The adsorption–desorption isotherms of TPC-S was a type IV isotherm loop, with a hysteresis loop in the  $P/P_0$  from 0.8 to 1.0, indicating that a mesoporous structure exists in the catalyst. The mesoporous structure in the TPC-S can offer active sites for conducting the reaction more effectively and improve the adsorption of substrates and the desorption ability of products, so as to better promote the reaction [33]. BJH analysis showed that the average pore diameter of TPC-S was 5.1 nm, with a specific surface area of 165.2 m<sup>2</sup>/g.

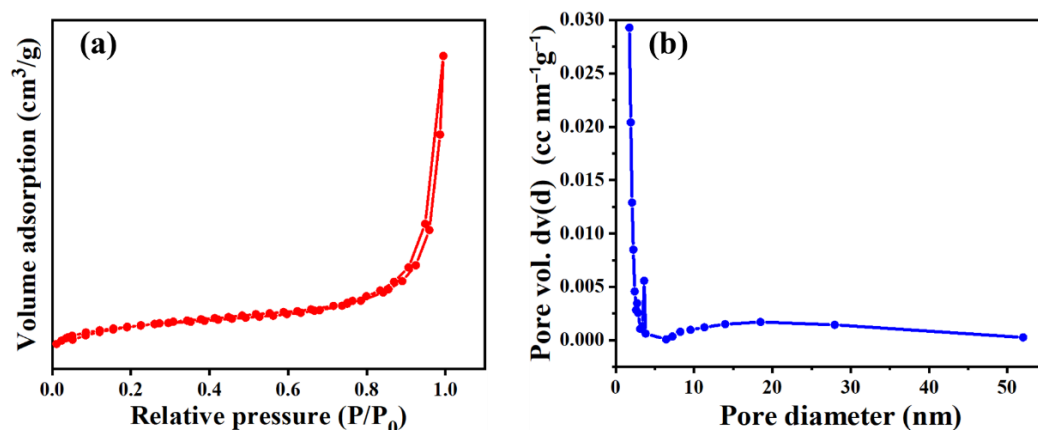


Figure 5. (a) The  $N_2$  adsorption–desorption isotherms and (b) pore size distribution of TPC-S.

The thermal stability of TPC-S was investigated by thermogravimetric (TG) analysis at 25–900 °C, as shown in Figure 6. According to the TG curve figure, the weight loss of TPC-S could be divided into three stages with increases in temperature. At 25–200 °C, there was a 6.1% weight loss for TPC-S, which could be attributed to the removal of a small amount of water adsorbed on TPC-S [34]. The second weight loss was 17.5% at 200–450 °C, due to the decomposition of  $-SO_3H$  groups into  $SO_2$  [35]. The final weight loss was 17% at 450–700 °C, which was the further decomposition of surface functional groups such as  $-OH$  and  $-COOH$  [36]. In addition, it is worth noting that TG analyses were carried out under a nitrogen atmosphere, with too much weight loss during the second and third stages. This is because the catalyst in this study was prepared by polymerization of aromatic monomers, during which oligomers (e.g., dimer and trimer) were formed. These oligomers were decomposed at 200–700 °C [37]. The catalyst was basically carbonized at a calcination temperature of >700 °C, resulting in a significant decrease in the pyrolysis rate. The TG curve of TPC-S showed that  $-SO_3H$  of the catalyst could be retained below 200 °C, which ensured that the reaction temperature would be within this range.

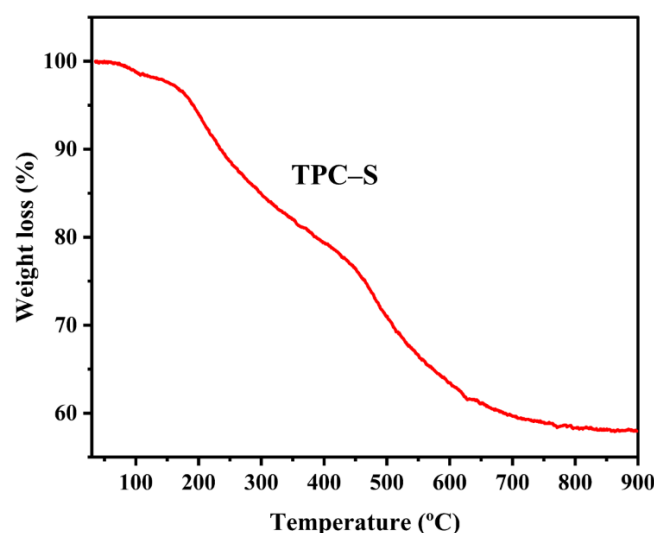


Figure 6. The TG curve of TPC-S.

## 2.2. Catalytic Reactions

### 2.2.1. Effect of Temperature and Time on EL Yield

The catalytic properties of TPC-S were estimated by the conversion of fructose into EL in the ethanol system. Firstly, the effects of reaction time on EL yields at different temperatures were studied. The reactions were carried out with 180 mg fructose and 50 mg

TPC-S in 5.0 mL ethanol at 90–170 °C for 4–15 h. As shown in Figure 7a, while the reaction temperature was maintained at 90–130 °C, the yields of EL increased rapidly with the increase of reaction temperature. High temperature promotes the formation of products attributed to atoms or molecules involved in the reaction at high temperatures, which are more likely to release or accept electrons [38]. Due to the complex conversion of fructose in ethanol, it involves a series-parallel reaction network (Scheme 1). It contains three main series-parallel chemical reactions: (a) fructose → HMF → LA → EL, (b) fructose → HMF → EMF → EL, and (c) fructose → ethyl-d-fructofuranoside (EDFF) → EMF → EL. Thus, 25.4%, 6.4%, and 0.8% yields of EMF were detected at 90, 110, and 130 °C, respectively, and 2.0% HMF was obtained at 90 °C. Furthermore, 48.5% and 22.4% yields of 5-(ethoxymethyl)furfural diethyl acetal (EMFdae) were detected at 90 and 110 °C, respectively. HMF, EMF, and EMFdae with furan rings are unstable at high temperatures, and further undergo ring-opening transformation into EL [39,40], which is one of the reasons for high EL yield at high temperatures. However, further steady increases in temperature (130–170 °C) had a faint influence on the yields of EL, and there was a slight decrease owing to the formation of humin and other by-products at higher temperatures [41]. Humin increased from 2.9% to 31.1% with increasing temperature. Furthermore, the by-product formic acid produced in the reaction system reacted with ethanol to form ethyl formate, which was also detected and increased from 8.2% to 25.1%. The optimal temperature for obtaining a high EL yield was found to be 130 °C. Therefore, the effect of time on the product formation was studied at 130 °C. As seen in Figure 7b, the yields of EL increased steadily to 70.3%, and the EMF yields decreased from 3.6% to 0.8% in 4–10 h. EMF was unstable at 130 °C and converted to EL over time. When the reaction time was prolonged from 10 to 15 h, the yield of EL decreased from 70.3 to 68.4%, while the amount of humin increased from 27.5 to 30.3%. Furthermore, during this period, the conversion of fructose was 100%. This can be attributed to the fact that more humin adhering to the catalyst surface with the extension of time inhibited the reaction activity [42], and the water formed in the reaction process led to the hydrolysis of the target product [25]. Overall, the optimum reaction time for EL yield was 10 h.

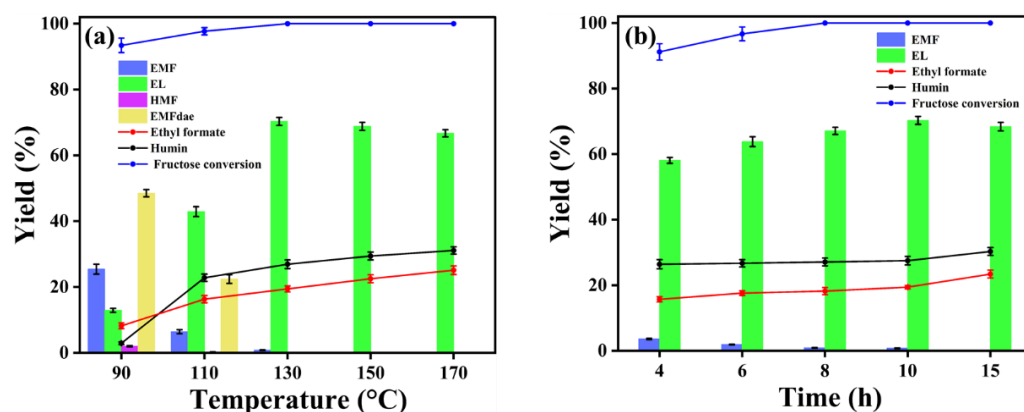
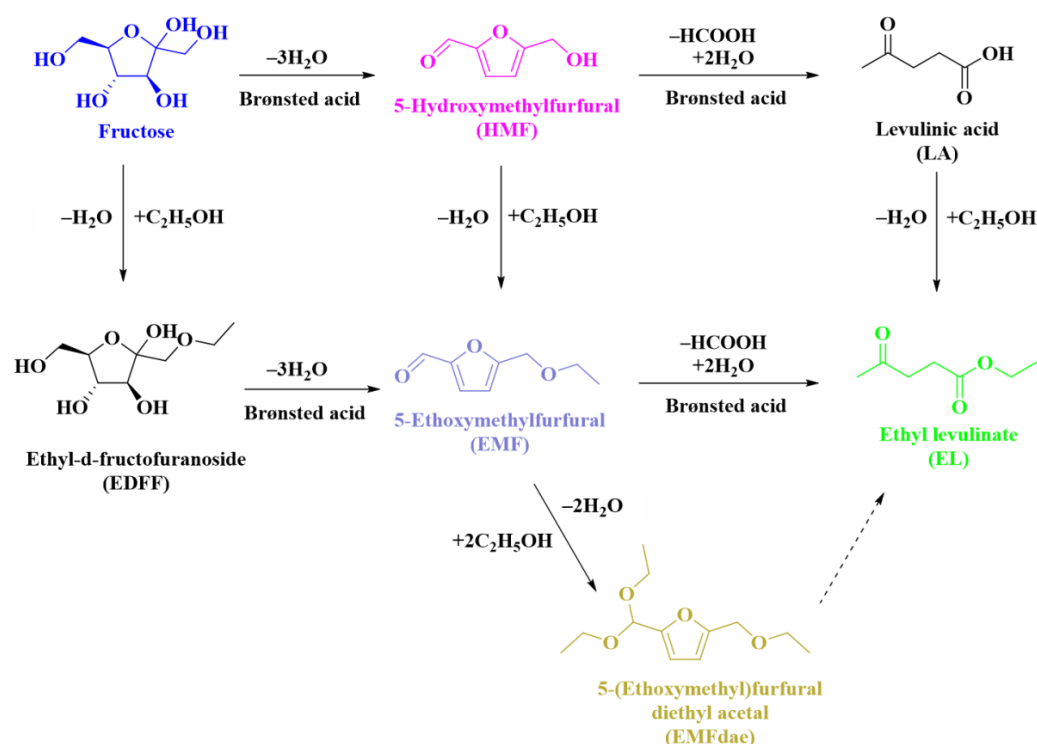


**Figure 7.** Effects of (a) reaction temperature (fructose 180 mg, TPC-S catalyst 50 mg, ethanol 5 mL, 10 h) and (b) reaction time (fructose 180 mg, TPC-S catalyst 50 mg, ethanol 5 mL, 130 °C) on EL yield.



**Scheme 1.** Schematic pathway of EL formation from fructose.

### 2.2.2. Effect of Fructose and Catalyst Dosage on EL Yield

The effect of fructose and catalyst dosages on the yield of EL is shown in Figure 8a,b. When the initial concentration of fructose was 36 g/L, the maximum EL yield (70.3%) could be obtained. At a low initial concentration (24 g/L), the yield of EL was 52.1%. Due to the low fructose concentration, there was excessive ethanol to compete with the catalyst active site ( $-\text{SO}_3\text{H}$ ) in the reaction system, which limited the protonation of the reactants [43]. When the initial concentration of fructose continued to increase to 48 g/L and 60 g/L, the EL yields decreased to 53.4% and 28.1%, respectively. This was due to the fact that fructose-to-EL conversion is a complex multi-step reaction involving multiple reaction intermediates, such as HMF, EMF, LA, and EDFF. Large numbers of fructose molecules compete for reactive sites. In the absence of active sites, these intermediates polymerize at high temperatures to form black insoluble (humin). Moreover, high fructose concentration will reduce the mass transfer rate of the reaction, thereby reducing the EL yield [41]. The amount of the catalyst also determines the yield of EL. In total, 64.3% EL was detected when the dosage of catalyst was 25 mg, and the yield increased to 70.3% when the dosage of the catalyst increased to 50 mg. However, when the dose was increased to 75 and 100 mg, the yield of EL declined to 69.3% and 68.1%, respectively. This phenomenon was determined by the number of catalytic active sites. Increasing the active sites (catalyst dosage) in an appropriate range can promote the reaction rate, but beyond this range, the number of active sites will no longer be a decisive factor in the reaction rate and even promote the occurrence of side reactions [44].

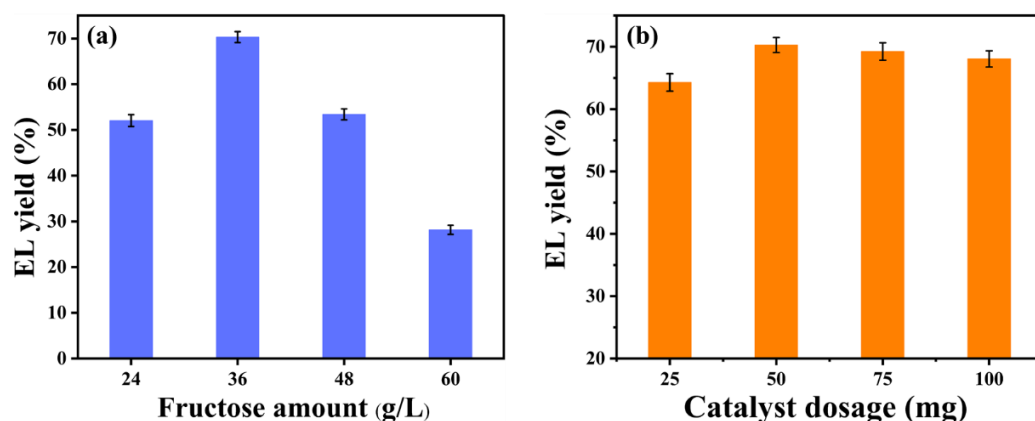


**Figure 8.** Effects of (a) fructose amount (catalyst 50 mg, ethanol 5 mL, 130 °C, 10 h) and (b) catalyst dosage (fructose 180 mg, ethanol 5 mL, 130 °C, 10 h) on EL yield.

### 2.2.3. Catalyst Reusability

According to the previous descriptions, the reaction was repeated for 10 h at 130 °C to study the reusability of TPC-S for EL preparation. As shown in Figure 9a, after four runs of TPC-S, the yield of EL decreased slightly from 70.3% to 65.6%, indicating that TPC-S had high stability. Most of its catalytic active sites were not leached after repeated use. This result can be confirmed by the FT-IR spectra (Figure 9b) before and after the use of the catalyst. Compared with the fresh catalyst, the C=O and C=C bond peaks of the catalyst gradually shifted after the first three uses. This is because a few of the products or byproducts adhered to the pore of the catalyst, altering the molecular interaction within the catalyst, thereby changing the chemical shift [31]. However, more shifts occurred after the fourth cycle due to more humin or other impurities adhering to the catalyst. Moreover, it was observed that the peak intensity corresponding to  $-\text{SO}_3\text{H}$  gradually decreased, which was owing to the leaching of a small amount of  $-\text{SO}_3\text{H}$  during the catalyst washing process. This was the cause of a slight decrease in EL yield.

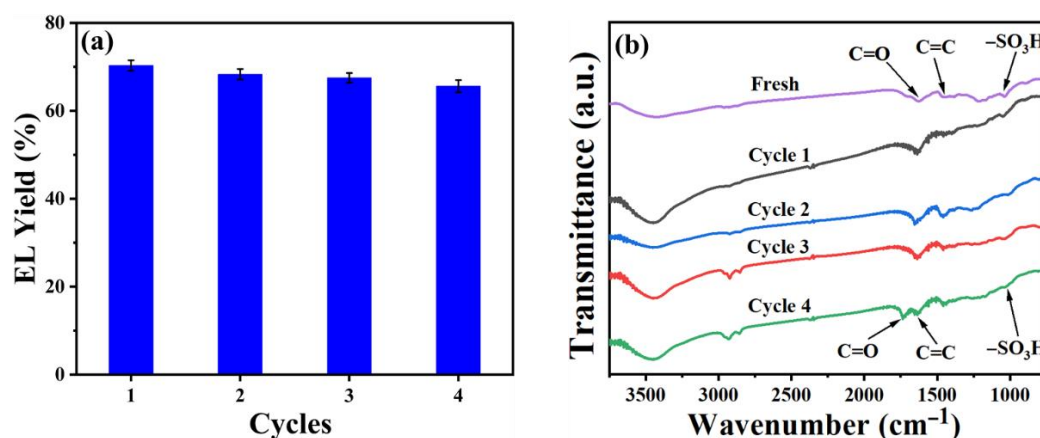


**Figure 9.** (a) Reusability study of TPC-S, and (b) FT-IR spectra of fresh and recycled TPC-S.

### 2.2.4. Comparison with Previous Catalytic Systems

In order to evaluate the advantages of our catalytic system in the synthesis of EL from fructose, the EL synthesis methods reported in this and previous studies are shown in Table 2. For example, the zeolite catalyst system usually requires a higher temperature and longer time and cannot obtain a satisfactory yield (Table 2, Entry 1). Table 2 (Entries 3–5) shows that the sulfonated carbon catalyst could obtain considerable EL yield (~55%). However, they needed a longer reaction time (Entry 3), a higher temperature, and a lower

S/C ratio (Entries 4 and 5). Therefore, the TPC-S catalyst prepared in this study had excellent catalytic performance.

**Table 2.** A comparison of the catalytic performance with previous work.

Entry	Substrate	Catalyst	S/C <sup>1</sup>	Temp (°C)	Time (h)	EL Yield (%)	Ref.
1	Fructose	H-USY (6)	1.7	160	20	40	[45]
2	Fructose	BioC-S3	2	130	6	28	[46]
3	Fructose	SO <sub>3</sub> H-SBA-15	3.4	140	24	57	[47]
4	Fructose	UCC-S-Fe-300	0.2	200	6	55.1	[25]
5	Fructose	Al/SBA-15	1	190	4	58	[48]
6	Fructose	TPC-S	3.6	130	10	70.3	This work

<sup>1</sup> The mass ratio of substrate and catalyst.

### 3. Materials and Methods

#### 3.1. Materials

Fructose (C<sub>6</sub>H<sub>12</sub>O<sub>6</sub>, 99%), 4-methylphenol (C<sub>7</sub>H<sub>8</sub>O, 99%), 4-ethylphenol (C<sub>8</sub>H<sub>10</sub>O, 97%), 4-propylphenol (C<sub>9</sub>H<sub>12</sub>O, ≥99%), ethyl levulinate (C<sub>7</sub>H<sub>12</sub>O<sub>3</sub>, 99%), naphthalene (C<sub>10</sub>H<sub>8</sub>, 99%), formaldehyde solution (HCHO, ≥36%), and iron(III) chloride (FeCl<sub>3</sub>, 99%) were all purchased from Macklin Biochemical Co., Ltd. (Shanghai, China). 1,2-dichloroethane (C<sub>2</sub>H<sub>4</sub>Cl<sub>2</sub>, 99%), ethanol (C<sub>2</sub>H<sub>5</sub>OH, ≥99.7%), and H<sub>2</sub>SO<sub>4</sub> (>98%) were purchased from InnoChem Science & Technology Co., Ltd. (Beijing, China). All reagents used here did not need further purification.

#### 3.2. Preparation of Catalysts

##### 3.2.1. Synthesis of TPC

TPC was synthesized by a phenolic condensation reaction. Briefly, the lignin monomer-derived phenols (4-methylphenol: 0.0012 mol, 4-ethylphenol: 0.0064 mol, and 4-propylphenol: 0.0124 mol) with a total mass of 0.02 mol were dissolved in 40 mL of 1,2-dichloroethane. Then 0.06 mol HCHO and 0.06 mol FeCl<sub>3</sub> were added. After stirring and refluxing for 5 h at 45 °C, the temperature was raised to 80 °C and continued to stir and reflux for 20 h. After that, the obtained solids were rinsed with anhydrous C<sub>2</sub>H<sub>5</sub>OH and dried overnight in a dry oven at 80 °C. Finally, brown ternary polymeric carbon (TPC) was obtained.

##### 3.2.2. Synthesis of TPC-S

TPC was mixed with 1,2-dichloroethane in a ratio of 1 g:10 mL, which was then slowly dripped with H<sub>2</sub>SO<sub>4</sub> (1 g TPC:30 mL H<sub>2</sub>SO<sub>4</sub>) and mixed at 80 °C for 4 h. Then, the residual 1,2-dichloroethane and H<sub>2</sub>SO<sub>4</sub> were washed with anhydrous C<sub>2</sub>H<sub>5</sub>OH until the pH of the eluent was 7, and the sulfonated TPC was obtained by overnight drying at 80 °C, which was denoted as TPC-S.

#### 3.3. Characterization

The structural information of TPC and TPC-S was obtained by a series of characterization techniques. XRD (X-ray diffraction) characterization was used to observe the crystal form of the catalysts, and the instrument model was Bruker D8 Advance, which uses Cu K $\alpha$  radiation with  $\lambda = 0.1548$  nm and  $2\theta$  ranging from 5° to 90°. Fourier transform infrared (FT-IR) spectra of the catalysts were measured by a NICOLET iS50 with a wavenumber range of 4000–500 cm<sup>-1</sup>, and spectral information was recorded by the KBr and tablet pressing method. X-ray photoelectron spectroscopy (XPS, Nexsa, Thermo Fisher Scientific, Waltham, MA, USA) was measured using an X-ray source of a monochromatic Al K $\alpha$  source, which was used to determine the chemical composition and combined state of the sample elements. The conditions of the high-resolution transmission electron microscope (HR-TEM) and elemental mapping were the same, and the instrument model was FEI TALOS F200C (Hillsboro, OR, USA). The surface morphology of the catalysts was detected

by scanning electron microscopy (SEM, Hitachi S-4800, Kyoto, Japan). Thermogravimetric analysis (TG) was carried out in a nitrogen medium at a heating rate of 10 °C/min with an STA 449F3 instrument at a temperature ranging from 25 °C to 900 °C. The surface area, pore volume, and pore size of the catalysts were tested by Brunauer–Emmett–Teller (BET, ASAP 2460, Atlanta, GA, USA). Ammonia temperature-programmed desorption (NH<sub>3</sub>-TPD, AutoChem 2920, Atlanta, GA, USA) was used to test the acid site distribution of the catalysts.

### 3.4. Catalytic Activity Evaluation

The reaction was completed in a 15 mL Teflon-lined stainless-steel autoclave (a magneton inside). The mixture contained 180 mg fructose, 25–100 mg catalyst, 5 mL ethanol, and naphthalene as internal standard. The reaction temperature was 90–170 °C, the reaction time was 4–15 h, and the speed was 600 rpm/min. After the reaction, cooling the reactor in flowing tap water stopped the reaction. Reaction liquid passed through a 0.22 µm filter, and the EL content was detected by gas chromatography (FID detector). The instrument model and column were Agilent 7890B (Agilent, Palo Alto, CA, USA) and HP-5 (30 m × 0.32 mm × 0.25 µm), respectively. Program: N<sub>2</sub> (1 mL/min), injection temperature 250 °C, detector temperature 300 °C, column temperature 60 °C. The heating program is 60 °C for 1 min, then raised from 60 to 230 °C (heating ramp: 10 °C/min), and kept at 230 °C for 5 min. The EL yield was calculated as follows:

$$\text{EL yield (\%)} = \frac{\text{Molar concentration of EL}}{\text{Initial molar concentration of fructose}} \times 100\%$$

## 4. Conclusions

In this study, a new type of heterogeneous ternary polymeric carbon catalyst was prepared by polymerization of three lignin monomers at a low temperature (80 °C). The catalyst had a layered structure (stacked by aromatic carbon polymerization) and mesoporous structure, with a BET-specific surface area of 165.2 m<sup>2</sup>/g and average pore size of 5.1 nm. A high specific surface area and an excellent layered structure provided more active sites (–SO<sub>3</sub>H), namely, high acid density (5.33 mmol/g). These features enabled TPC–S to effectively catalyze the conversion of fructose (initial concentration 36 g/L) to EL (70.3% yield) at 130 °C for 10 h. Furthermore, the reusability of TPC–S was studied, and its catalytic activity decreased slightly after four cycles (from 70.3% to 65.6%), which indicated that the cheap catalysts prepared from renewable raw materials with great stability show great potential for the conversion of biomass to valuable chemicals.

**Author Contributions:** Conceptualization, D.Y. and X.L.; methodology, H.L. (Hangyu Luo); software, J.H.; formal analysis, J.H. and H.L. (Hangyu Luo); investigation, D.Y.; resources, X.L. and H.L. (Hu Li); writing—original draft preparation, D.Y.; writing—review and editing, X.L. and H.L. (Hu Li); supervision, X.L. and H.L. (Hu Li). All authors have read and agreed to the published version of the manuscript.

**Funding:** This research was funded by the Technical Talent Support Program of Guizhou Education Department ([2022]087), the scientific research funds of Guiyang University (GYU-KY-[2022]), the Guizhou Provincial Key Laboratory for Rare Animal and Economic Insects of the Mountainous Region ([2018]5102), Guizhou Provincial S&T Project (ZK[2022]011), and the National Natural Science Foundation of China (21908033, 22065004).

**Data Availability Statement:** The data presented in this study are available on request from the corresponding author.

**Conflicts of Interest:** The authors declare no conflict of interest.

## References

1. Abraham, A.; Mathew, A.K.; Park, H.; Choi, O.; Sindhu, R.; Parameswaran, B.; Pandey, A.; Park, J.H.; Sang, B.-I. Pretreatment strategies for enhanced biogas production from lignocellulosic biomass. *Bioresour. Technol.* **2020**, *301*, 122725. [[CrossRef](#)] [[PubMed](#)]
2. Li, H.; Yang, S.; Riisager, A.; Pandey, A.; Sangwan, R.S.; Saravanamurugan, S.; Luque, R. Zeolite and zeotype-catalysed transformations of biofuranic compounds. *Green Chem.* **2016**, *18*, 5701–5735. [[CrossRef](#)]
3. Martirena, F.; Monzó, J. Vegetable ashes as supplementary cementitious materials. *Cement Concrete Res.* **2018**, *114*, 57–64. [[CrossRef](#)]
4. Liu, J.; Li, H.; Liu, Y.-C.; Lu, Y.-M.; He, J.; Liu, X.-F.; Wu, Z.-B.; Yang, S. Catalytic conversion of glucose to 5-hydroxymethylfurfural over nano-sized mesoporous Al<sub>2</sub>O<sub>3</sub>–B<sub>2</sub>O<sub>3</sub> solid acids. *Catal. Commun.* **2015**, *62*, 19–23. [[CrossRef](#)]
5. Li, H.; Li, Y.; Fang, Z.; Smith, R.L., Jr. Efficient catalytic transfer hydrogenation of biomass-based furfural to furfuryl alcohol with recyclable Hf-phenylphosphonate nanohybrids. *Catal. Today* **2019**, *319*, 84–92. [[CrossRef](#)]
6. Li, H.; Zhang, Q.; Bhadury, P.; Yang, S. Furan-type compounds from carbohydrates via heterogeneous Catalysis. *Curr. Org. Chem.* **2014**, *18*, 547–597. [[CrossRef](#)]
7. Li, H.; He, X.; Zhang, Q.; Chang, F.; Xue, W.; Zhang, Y.; Yang, S. Polymeric ionic hybrid as solid acid catalyst for the selective conversion of fructose and glucose to 5-hydroxymethylfurfural. *Energy Technol.* **2013**, *1*, 151–156. [[CrossRef](#)]
8. Kumari, N.; Chhabra, T.; Kumar, S.; Krishnan, V. Nanoarchitectonics of sulfonated biochar from pine needles as catalyst for conversion of biomass derived chemicals to value added products. *Catal. Commun.* **2022**, *168*, 106467. [[CrossRef](#)]
9. Guo, H.; Hirotsaki, Y.; Qi, X.; Smith, R.L., Jr. Synthesis of ethyl levulinate over amino-sulfonated functional carbon materials. *Renew. Energy* **2020**, *157*, 951–958. [[CrossRef](#)]
10. Windom, B.C.; Lovestead, T.M.; Mascal, M.; Nikitin, E.B.; Bruno, T.J. Advanced distillation curve analysis on ethyl levulinate as a diesel fuel oxygenate and a hybrid biodiesel fuel. *Energy Fuels* **2011**, *25*, 1878–1890. [[CrossRef](#)]
11. Unlu, D.; Boz, N.; Ilgen, O.; Hilmioglu, N. Improvement of fuel properties of biodiesel with bioadditive ethyl levulinate. *Open Chem.* **2018**, *16*, 647–652. [[CrossRef](#)]
12. Ji, N.; Diao, X.; Yu, Z.; Liu, Z.; Jiang, S.; Lu, X.; Song, C.; Liu, Q.; Ma, D.; Liu, C. Catalytic transfer hydrogenation of ethyl levulinate to  $\gamma$ -valerolactone over supported MoS<sub>2</sub> catalysts. *Catal. Sci. Technol.* **2021**, *11*, 5062–5076. [[CrossRef](#)]
13. Ogino, I.; Suzuki, Y.; Mukai, S.R. Esterification of levulinic acid with ethanol catalyzed by sulfonated carbon catalysts: Promotional effects of additional functional groups. *Catal. Today* **2018**, *314*, 62–69. [[CrossRef](#)]
14. Gupta, S.S.R.; Kantam, M.L. Catalytic conversion of furfuryl alcohol or levulinic acid into alkyl levulinates using a sulfonic acid-functionalized hafnium-based MOF. *Catal. Commun.* **2019**, *124*, 62–66. [[CrossRef](#)]
15. Silva, J.F.L.; Maciel, M.R.W.; Maciel Filho, R. Optimization of high temperature reactive distillation for production of ethyl levulinate. *Chem. Eng. Trans.* **2018**, *69*, 379–384. [[CrossRef](#)]
16. Le Van Mao, R.; Zhao, Q.; Dima, G.; Petraccone, D. New process for the acid-catalyzed conversion of cellulosic biomass (ac3b) into alkyl levulinates and other esters using a unique one-pot system of reaction and product extraction. *Catal. Lett.* **2010**, *141*, 271–276. [[CrossRef](#)]
17. Chang, C.; Xu, G.; Jiang, X. Production of ethyl levulinate by direct conversion of wheat straw in ethanol media. *Bioresour. Technol.* **2012**, *121*, 93–99. [[CrossRef](#)] [[PubMed](#)]
18. Heda, J.; Niphadkar, P.; Mudliar, S.; Bokade, V. Highly efficient micro-meso acidic H-USY catalyst for one step conversion of wheat straw to ethyl levulinate (biofuel additive). *Micropor. Mesopor. Mater.* **2020**, *306*, 110474. [[CrossRef](#)]
19. Lai, F.; Yan, F.; Wang, P.; Qu, F.; Shen, X.; Zhang, Z. Efficient one-pot synthesis of ethyl levulinate from carbohydrates catalyzed by Wells-Dawson heteropolyacid supported on Ce–Si pillared montmorillonite. *J. Clean. Prod.* **2021**, *324*, 129276. [[CrossRef](#)]
20. Li, H.; Fang, Z.; Smith, R.L., Jr.; Yang, S. Efficient valorization of biomass to biofuels with bifunctional solid catalytic materials. *Prog. Energy Combust.* **2016**, *55*, 98–194. [[CrossRef](#)]
21. Li, X.; Li, Y.; Wang, X.; Peng, Q.; Hui, W.; Hu, A.; Wang, H. Zr-DBS with sulfonic group: A green and highly efficient catalyst for alcoholysis of furfuryl alcohol to ethyl levulinate. *Catal. Lett.* **2021**, *151*, 2622–2630. [[CrossRef](#)]
22. Tian, H.; Shao, Y.; Liang, C.; Xu, Q.; Zhang, L.; Zhang, S.; Liu, S.; Hu, X. Sulfated attapulgite for catalyzing the conversion of furfuryl alcohol to ethyl levulinate: Impacts of sulfonation on structural transformation and evolution of acidic sites on the catalyst. *Renew. Energy* **2020**, *162*, 1576–1586. [[CrossRef](#)]
23. Lv, Z.; Xu, J.; Li, C.; Dai, L.; Li, H.; Zhong, Y.; Si, C. pH-Responsive lignin hydrogel for lignin fractionation. *ACS Sustain. Chem. Eng.* **2021**, *9*, 13972–13978. [[CrossRef](#)]
24. Na, W.; Qu, Z.; Chen, X.; Su, X. A turn-on fluorescent probe for sensitive detection of sulfide anions and ascorbic acid by using sulfanilic acid and glutathione functionalized graphene quantum dots. *Sens. Actuators B-Chem.* **2018**, *256*, 48–54. [[CrossRef](#)]
25. Zainol, M.M.; Asmadi, M.; Iskandar, P.; Ahmad, W.A.N.W.; Amin, N.A.S.; Hoe, T.T. Ethyl levulinate synthesis from biomass derivative chemicals using iron doped sulfonated carbon cryogel catalyst. *J. Clean. Prod.* **2021**, *281*, 124686. [[CrossRef](#)]
26. Li, T.; Shen, S.; Cai, B.; Wang, Y.; Peng, X.; Li, Y. High-performance carbon-based solid acid prepared by environmental and efficient recycling of PVC waste for cellulose hydrolysis. *RSC Adv.* **2016**, *6*, 91921–91929. [[CrossRef](#)]
27. Huang, Z.; Hao, S.; Yuan, H. Synthesis of ethyl levulinate from cellulose over a double acid site catalyst. *J. Chem. Technol. Biot.* **2021**, *97*, 240–253. [[CrossRef](#)]
28. Huang, M.; Luo, J.; Fang, Z.; Li, H. Biodiesel production catalyzed by highly acidic carbonaceous catalysts synthesized via carbonizing lignin in sub- and super-critical ethanol. *Appl. Catal. B Environ.* **2016**, *190*, 103–114. [[CrossRef](#)]

29. Xiao, H.; Guo, Y.; Liang, X.; Qi, C. One-step synthesis of novel biacidic carbon via hydrothermal carbonization. *J. Solid State Chem.* **2010**, *183*, 1721–1725. [[CrossRef](#)]
30. Chen, Y.; Guan, W.; Zhang, Y.; Yan, C.; Li, B.; Wei, Y.; Pan, J.; Yan, Y. One-Pot synthesis of the biofuel 5-ethoxymethylfurfural from carbohydrates using a bifunctional catalyst prepared through a pickering hipec template and pore-filled strategy. *Energy Fuels* **2020**, *34*, 14264–14274. [[CrossRef](#)]
31. Huang, J.; Jian, Y.; Li, H. A New lamellar biocarbon catalyst with enhanced acidity and contact sites for efficient biodiesel production. *Waste Biomass Valorization* **2022**, *13*, 1–16. [[CrossRef](#)]
32. Kuang, P.; Sayed, M.; Fan, J.; Cheng, B.; Yu, J. 3D Graphene-based H<sub>2</sub>-production photocatalyst and electrocatalyst. *Adv. Energy Mater.* **2020**, *10*, 1903802. [[CrossRef](#)]
33. Zhong, Y.; Deng, Q.; Yao, Q.; Lu, C.; Zhang, P.; Li, H.; Wang, J.; Zeng, Z.; Zou, J.-J.; Deng, S. Functionalized biochar with superacidity and hydrophobicity as a highly efficient catalyst in the synthesis of renewable high-density fuels. *ACS Sustain. Chem. Eng.* **2020**, *8*, 7785–7794. [[CrossRef](#)]
34. Ayashi, N.; Chermahini, A.N.; Saraji, M. Biomass conversion to alkyl levulinates using heteropoly acid carbon mesoporous composites. *Process Saf. Environ.* **2022**, *160*, 988–1000. [[CrossRef](#)]
35. Bastos, R.R.C.; da Luz Corrêa, A.P.; da Luz, P.T.S.; da Rocha Filho, G.N.; Zamian, J.R.; da Conceição, L.R.V. Optimization of biodiesel production using sulfonated carbon-based catalyst from an amazon agro-industrial waste. *Energy Convers. Manag.* **2020**, *205*, 112457. [[CrossRef](#)]
36. Zhang, M.; Sun, A.; Meng, Y.; Wang, L.; Jiang, H.; Li, G. High activity ordered mesoporous carbon-based solid acid catalyst for the esterification of free fatty acids. *Micropor. Mesopor. Mater.* **2015**, *204*, 210–217. [[CrossRef](#)]
37. Liudvinavičiūtė, D.; Rutkaite, R.; Bendoraitienė, J.; Klimavičiūtė, R. Thermogravimetric analysis of caffeic and rosmarinic acid containing chitosan complexes. *Carbohydr. Polym.* **2019**, *222*, 115003. [[CrossRef](#)]
38. Ramli, N.A.S.; Amin, N.A.S. Fe/HY zeolite as an effective catalyst for levulinic acid production from glucose: Characterization and catalytic performance. *Appl. Catal. B Environ.* **2015**, *163*, 487–498. [[CrossRef](#)]
39. Li, H.; Saravanamurugan, S.; Yang, S.; Riisager, A. Direct transformation of carbohydrates to the biofuel 5-ethoxymethylfurfural by solid acid catalysts. *Green Chem.* **2016**, *18*, 726–734. [[CrossRef](#)]
40. Liu, X.; Yu, D.; Luo, H.; Li, C. Catalytic upgrading of lignocellulosic biomass sugars toward biofuel 5-ethoxymethylfurfural. *Front. Chem.* **2022**, *9*, 831102. [[CrossRef](#)]
41. Tian, L.; Zhang, L.; Liu, Y.; He, Y.; Zhu, Y.; Sun, R.; Yi, S.; Xiang, J. Clean production of ethyl levulinate from kitchen waste. *J. Clean. Prod.* **2020**, *268*, 122296. [[CrossRef](#)]
42. Heda, J.N.; Niphadkar, P.S.; Bokade, V.V. Efficient synergetic combination of h-usy and sno2 for direct conversion of glucose into ethyl levulinate (biofuel additive). *Energy Fuels* **2019**, *33*, 2319–2327. [[CrossRef](#)]
43. Dhawane, S.H.; Karmakar, B.; Ghosh, S.; Halder, G. Parametric optimisation of biodiesel synthesis from waste cooking oil via Taguchi approach. *J. Environ. Chem. Eng.* **2018**, *6*, 3971–3980. [[CrossRef](#)]
44. Chen, B.; Xu, G.; Zheng, Z.; Wang, D.; Zou, C.; Chang, C. Efficient conversion of corn stover into 5-ethoxymethylfurfural catalyzed by zeolite USY in ethanol/THF medium. *Ind. Crops Prod.* **2019**, *129*, 503–511. [[CrossRef](#)]
45. Saravanamurugan, S.; Riisager, A. Zeolite catalyzed transformation of carbohydrates to alkyl levulinates. *ChemCatChem* **2013**, *5*, 1754–1757. [[CrossRef](#)]
46. Peixoto, A.F.; Ramos, R.; Moreira, M.M.; Soares, O.S.G.; Ribeiro, L.S.; Pereira, M.F.; Delerue-Matos, C.; Freire, C. Production of ethyl levulinate fuel bioadditive from 5-hydroxymethylfurfural over sulfonic acid functionalized biochar catalysts. *Fuel* **2021**, *303*, 121227. [[CrossRef](#)]
47. Saravanamurugan, S.; Riisager, A. Solid acid catalysed formation of ethyl levulinate and ethyl glucopyranoside from mono- and disaccharides. *Catal. Commun.* **2012**, *17*, 71–75. [[CrossRef](#)]
48. Babaei, Z.; Chermahini, A.N.; Dinari, M. Alumina-coated mesoporous silica SBA-15 as a solid catalyst for catalytic conversion of fructose into liquid biofuel candidate ethyl levulinate. *Chem. Eng. J.* **2018**, *352*, 45–52. [[CrossRef](#)]